



Multi-wavelength lock-in spectroscopy for extracting perturbed spectral responses: molecular signatures in nanocavities

ANGELOS XOMALIS^{1,2,3}  AND JEREMY J. BAUMBERG^{1,*} 

¹NanoPhotonics Centre, Cavendish Laboratory, Department of Physics, University of Cambridge, Cambridge CB3 0HE, United Kingdom

²Empa, Swiss Federal Laboratories for Materials Science and Technology, Laboratory for Mechanics of Materials and Nanostructures, Thun 3602, Switzerland

³Angelos.Xomalis@empa.ch

*jjb12@cam.ac.uk

Abstract: Detecting small changes in spectral fingerprints at multiple wavelength bands simultaneously is challenging for many spectroscopic techniques. Because power variations, drift, and thermal fluctuations can affect such measurements on different timescales, high speed lock-in detection is the preferred method, however this is typically a single channel (wavelength) technique. Here, a way to achieve multichannel (multi-wavelength) lock-in vibrational spectroscopy is reported, using acousto-optic modulators to convert nanosecond periodic temporal perturbations into spatially distinct spectra. This simultaneously resolves perturbed and reference spectra, by projecting them onto different locations of the spectrometer image. As an example, we apply this multichannel time-resolved methodology to detect molecular frequency upconversion in plasmonic nanocavities from the perturbed Raman scattering at different wavelengths. Our phase-sensitive detection scheme can be applied to any spectroscopy throughout the visible and near-infrared wavelength ranges. Extracting perturbed spectra for measurements on nanosecond timescales allows for capturing many processes, such as semiconductor optoelectronics, high-speed spectro-electrochemistry, catalysis, redox chemistry, molecular electronics, or atomic diffusion across materials.

Published by Optica Publishing Group under the terms of the [Creative Commons Attribution 4.0 License](https://creativecommons.org/licenses/by/4.0/). Further distribution of this work must maintain attribution to the author(s) and the published article's title, journal citation, and DOI.

1. Introduction

Interrogation of materials or molecules by light reveals a vast range of information. Frequently what is of interest is how these optical properties change on perturbing the system, for instance with electric fields, optical irradiation, magnetic field or other externally imposed variables. When the resulting changes are large, it is simply best to compare spectra before and after the perturbation is applied. However in situations where the perturbation is weak (<1%), then intrinsic low frequency noise such as sample drift, slow degradation, or heating is superimposed on the looked-for changes making their extraction problematic. To solve this problem, typically the perturbation is rapidly turned on and off, and a single-channel detection (for instance at a specific detection wavelength) is used together with lock-in measurement that extracts the in-phase quadrature of the signal. To obtain the perturbed spectra, this single-channel detection is scanned in wavelength. However again slow changes confound these slow scans, giving unreliable perturbed spectra.

Here we describe a general method that can overcome this constraint in any spectroscopy. It uses acousto-optic deflection to send the detected spectrum to two different regions of a spectrometer CCD camera depending on whether the perturbation is on or off. Since deflection

speeds reach 1 ns, while CCDs support more than 16-bit resolution per pixel, this gives stable time-integrated signals for both the perturbed and unperturbed spectra. Previous approaches using switchable charge reservoirs for linear photodetector arrays [1,2] suffered from the need to create bespoke detectors (rather than using optimized scientific grade CCDs), and restrictions on modulation speeds to <10 Hz which is too slow to eliminate most low frequency noise.

To demonstrate how this scheme works, we apply it to the surface-enhanced Raman scattering (SERS) of plasmonic constructs which allow for probing only tens of molecules. Light-matter interactions in such plasmonic nanocavities deliver SERS enhancements of order 10^9 and provide sensitivities hard to obtain with any other spectroscopic technique [3–7]. Such light confinement leads to observation of a wide range of phenomena under ambient conditions such as enhanced analytic spectroscopies [8,9], ultrafast spontaneous emission [10], lasing [11], and ultra-strong coupling [12].

Low frequency confounding signals are typically problematic. For instance, here the extreme light localisation initiates atomic migration/dislocation [13], and optical driving produces adatom ‘picocavities’ [14], accelerates dye bleaching, drives plasmonic chemistry [15,16], besides other events. Nanoscale spectroscopies often require high-precision nano-positioning giving unstable signals under thermal or mechanical drift (Fig. 1). Thus such experiments demonstrate well the key requirement to distinguish changes in molecular signals from intrinsic phenomena due to extraneous factors.

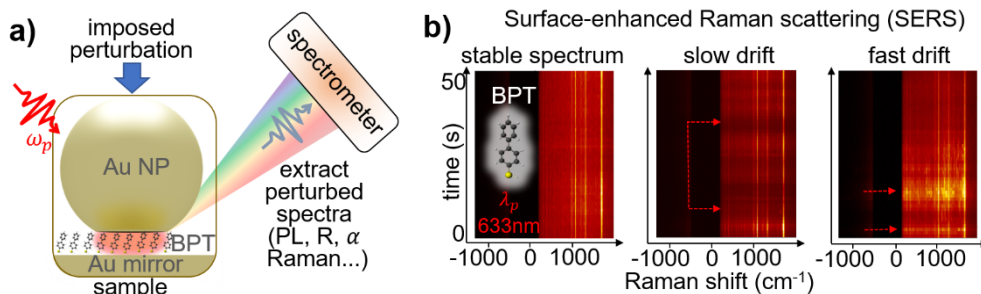


Fig. 1. Imposed spectral perturbation on a sample. a) Schematic of detected spectra from sample. Example sample here is a plasmonic nano-gap formed from gold nanoparticle (NP) deposited on self-assembled monolayer of biphenyl-4-thiol (BPT) coating a flat Au mirror. b) Consecutive SERS spectra over 50 s, showing in different cases a stable spectrum, or exhibiting slow or fast spectral drift (arrows).

2. Results and discussion

One rationale for probing a molecular nanogap system is its ability to detect mid-infrared (MIR) light. In this case, the periodic perturbation is MIR incident light which is tuned to be absorbed by a vibration in biphenyl-4-thiol (BPT) molecules. These are embedded in a plasmonic nanogap between nanoparticle (NP) and mirror, the latter patterned into a MIR resonator. This device is hence termed a NP-on-resonator (NPoR), and the spectrum measured is SERS pumped by an additional 785 nm laser, which increases when MIR light is absorbed [17]. We note many other modalities are generally also possible such as perturbed hyperspectral imaging [18,19], photothermally-modulated fluorescence [20,21] or vibrationally-assisted luminescence [22]. In all cases however, the limit of detection is set by the smallest possible change in the spectrum that can be observed.

Conventionally, lock-in-based detection techniques resolve small signal variations within a larger background plus noise. Small changes are hard to resolve in successive spectra taken

with the perturbation on or off, while lock-in detection operates at a single wavelength (grey dashed line, Fig. 2(a)). To measure perturbed and reference spectra directly, we develop a multichannel lockin-‘free’ spectroscopic technique. By switching a detection acousto-optic modulator (detAOM) at the same modulation speed as the perturbation, the different diffraction orders 0,1 collect different fractions of the perturbed and reference spectra. The imaging optics and wavelength-dependent diffraction then produce characteristic tilted spectra on the spectrometer CCD (Fig. 2(b)). These can be calibrated and analysed to reconstruct perturbed and reference spectra. The wavelength-dependent diffraction angles generated by the acoustic grating inside the AOM lead to different incident angles onto the front slit of the spectrometer and then onto the spectrometer grating, which leads to the tilted spectra. A wedge prism alignment allows this tilted pattern to be shifted into the optimal orientation away from the undiffracted beam. By changing the phase of the AOM drive frequency compared to the modulated perturbation, full phase-sensitive lock-in detection can be achieved.

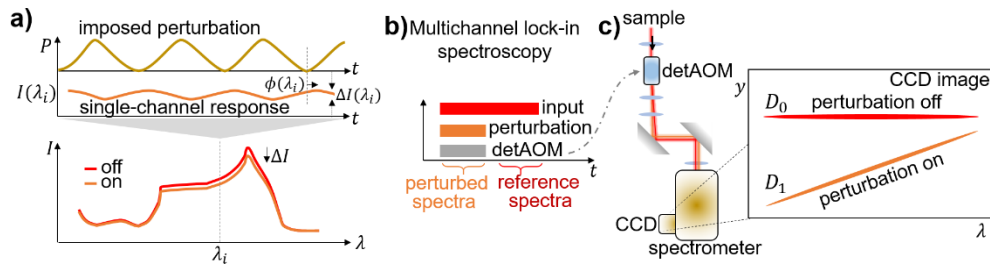


Fig. 2. Wavelength-resolved multichannel lock-in spectroscopy. a) Imposed periodic perturbation in time (top) results in spectral signal intensity changes $\Delta I(\lambda_i)$ (bottom), that can be measured using single-channel (wavelength) lock-in (grey, centred at λ_i). However it is desirable to measure the induced perturbation across a wide range of wavelengths (bottom, orange), but challenging to implement with standard single-wavelength lock-in methodologies. b) Implementation of multi-channel lock-in: timing sequence for each repetition cycle showing input laser (red), imposed perturbation (orange) and detection acousto-optic modulator (detAOM, grey). c) detAOM separates reference and perturbed spectra into 0th (D_0) and 1st (D_1) diffraction orders, which are mapped onto different vertical positions y of the spectrometer CCD.

In the example developed here, we study molecular fingerprints via SERS within the NPoR doubly frequency resonant antenna. Photolithography is used to fabricate 6 μm diameter Au disks of 100 nm thickness, which are coated by a BPT monolayer and then sandwiched by 60 nm Au nanoparticles. This creates a metal-dielectric-metal nanocavity of width set by the molecule length (here ~ 1.3 nm, Fig. 1(a)). The NPoR confines visible/near-infrared (NIR) and MIR light within the same active region below the NP [23], allowing strong optomechanical coupling and nonlinearities [17,24,25]. Frequency upconversion is predicted for the $\nu = 1080\text{cm}^{-1}$ BPT mode which is both IR and Raman active [26], and is seen as a SERS increase when pumped with IR light of this frequency (Fig. 3(a)) [17].

An optical microscope is used with synchronized illumination from NIR (ω_p) probe and IR (ω_{IR}) pump beams focusing via separate microscope objectives onto single nanostructures. Rectangular pulses of $\lambda_p = 785$ nm pump (0.4 μs) and $\lambda = 9.3$ μm probe (0.2 μs) light from a tuneable quantum cascade laser (QCL) are produced via synced signal function generators (SG) driving a pair of AOMs installed in illumination and detection arms (Fig. 2(b), 3(b)). This temporal sequence (Fig. 3(b)) repeats every 5 μs (0.2 MHz, limited by QCL drive electronics). With the detection AOM (detAOM) off, perturbed and reference spectra are both at 0th order

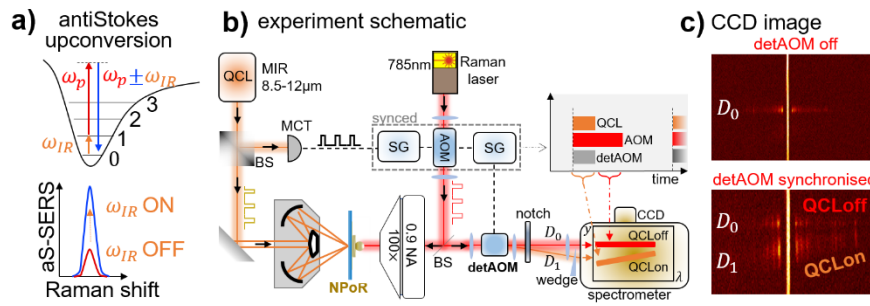


Fig. 3. Frequency upconversion of infrared to visible photons in dual resonant antennas. a) Upconversion process showing increase of SERS signal in sidebands ($\omega_p \pm \omega_{IR}$) of the Raman probe laser (ω_p) upon infrared (IR) pump (ω_{IR}) irradiation. b) Dual band microscope superimposes visible probe and IR pump radiation on doubly resonant antennas (nanoparticle-on-resonator, NPoR) for molecular frequency upconversion: AOM (probe acousto-optic modulator), detAOM (detection acousto-optic modulator), MCT (mercury-cadmium-telluride detector), BS (beam splitter), SG (signal generator). c) SERS spectra of BPT in the D_0 and D_1 diffraction orders when detAOM and laser AOM are synchronized (bottom) or detAOM off (top).

(D_0 , Fig. 3(c) top). By contrast, adjusting the time sequence results in perturbed spectra (orange, QCLon) only in 1st order (D_1) with reference spectra (red, QCLoff) only in 0th order (D_0).

Analysis of the CCD images reconstructs the desired spectra (Fig. 4(a)). Raman scattered light from the sample (with laser light removed using notch filters) is focused into the detAOM, and when the acoustic grating on, this is diffracted with near 60% efficiency into the 1st order. Separation of the two orders is achieved by inserting a 5° wedge prism before the spectrometer entrance slit. The 0th order contains both light when the detAOM is off (synchronized to when the QCL is off) and the residual (~40%) when the detAOM is on. The exact efficiencies can be normalized out using scattered pump light with the notch filter removed. The spectra within each box (Fig. 4(a)) are then binned (using the tilted geometry as shown), background subtracted, and corrected (see Supplement 1 Section 1). This retrieves the true perturbed (S_1) and reference (S_0) spectra (Fig. 4(b)). We note that the tilted pattern of D_1 occurs due to the angle of incidence of this diffraction order into the spectrometer gratings that is a few degrees off normal.

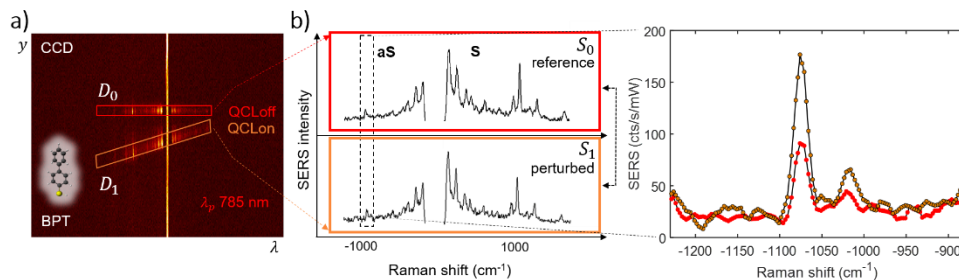


Fig. 4. Multichannel spectroscopy for extracting perturbed molecular signatures in nanocavities. a) Diffracted order D_0 (D_1) corresponds to infrared pump laser off (on) state. b) Correlation of S_0 and S_1 spectra allows the detection of SERS signal changes in multiple wavelength bands.

In the example here, multichannel spectroscopy detects the molecular frequency upconversion as discussed above [26]. With the QCL laser tuned to pump the $\nu = 1080 \text{ cm}^{-1}$ BPT vibration

while measuring SERS via the NIR probe beam, frequency upconversion is seen as an increase of the anti-Stokes in D_1 . To validate the effect of IR pumping, we compare the perturbed spectrum of S_1 with the reference S_0 (no IR) and find a 100% increase of the anti-Stokes SERS signal for QCL input average power of $5 \mu\text{W}/\mu\text{m}^2$ (orange, Fig. 4(c)). With this technique we are able to resolve changes $<5\%$ despite considerable drift in the SERS spectra. Our lock-in detection technique has response speeds $<1\mu\text{s}$ (set by the QCL pulse duration) which is far faster than power variations, drift, and thermal fluctuation timescales.

As noted, this spectroscopy is not limited to SERS, but can encompass any modality including reflection, transmission, absorption, scattering, photoluminescence and more. A wide range of periodic perturbations can be accommodated including voltages, thermal pulses, and electric or magnetic fields. Any spectral range accessed by the spectrometer gratings can be utilized, although the distortions from chromatic optics may require more sophisticated spatial corrections for larger bandwidths. Calibration is however systematic and straightforward. The ultimate speed is limited by how tightly the collected emission can be refocussed onto the AOM acoustic diffraction grating (for the exemplar here, the light emerges from a diffraction-limited spot), reaching eventually the maximum modulation speed of the AOM (typically as fast as 10 ns).

Intrinsically the technique developed here shifts the phase-sensitive signal detection to high frequencies which decreases all $1/f$ noise sources, without introducing additional noise. Signal sensitivity limitations relate to the charge well-depth of CCD pixels (often now $1:10^5$), although this can be avoided by using additional cylindrical lenses to vertically blur the spectra over more pixels on the CCD image, as well as to the pixel dark noise (often very low, $\sim 10^{-4}/\text{pixel/s}$). This multichannel lock-in spectroscopy module excludes all slow drifts and can be simply implemented in most spectroscopy configurations. It is thus of wide interest across fields from photochemistry to quantum physics.

3. Conclusions

We demonstrate a multichannel lock-in spectroscopic technique to extract perturbed spectral signatures. We show how diffracting the collected light from a sample into different spectra projected onto a spectrometer CCD camera simultaneously records reference and perturbed spectra. Since the AOMs have sub-microsecond resolution, it allows extraction of small perturbations and eliminates slower signal intensity fluctuations deriving from external factors. We use a plasmonic nanocavity sample to exemplify the feasibility of this technique, identifying upconversion in a molecular optomechanical signature. Our multichannel method is ideal for detecting spectral intensity variations at any wavelength and may be used to track a wide variety of nonlinear spectroscopic effects. We note that even faster modulation is possible by instead using polarization separation on the CCD via electro-optic modulators.

Funding. Engineering and Physical Sciences Research Council (EP/L015978/1, EP/L027151/1, EP/P029426/1, EP/R020965/1, EP/S022953/1); European Research Council (829067, 861950, 883703); Eidgenössische Materialprüfungs- und Forschungsanstalt (IRC 2021).

Acknowledgments. We acknowledge support from Empa internal funding call (IRC 2021), European Research Council (ERC) under Horizon 2020 research and innovation programme THOR (829067), POSEIDON (861950) and PICOFORCE (883703). We acknowledge funding from the EPSRC (Cambridge NanoDTC EP/L015978/1, EP/L027151/1, EP/S022953/1, EP/P029426/1, and EP/R020965/1).

Disclosures. The authors declare no conflicts of interest.

Data availability. All data used for the figures are available upon reasonable request from the corresponding author.

Supplemental document. See [Supplement 1](#) for supporting content.

References

1. R. J. Smith, R. A. Light, S. D. Sharples, N. S. Johnston, M. C. Pitter, and M. G. Somekh, "Multichannel, time-resolved picosecond laser ultrasound imaging and spectroscopy with custom complementary metal-oxide-semiconductor detector," *Rev. Sci. Instrum.* **81**(2), 024901 (2010).
2. P. Farah, A. Demetriadou, S. Salvatore, S. Vignolini, M. Stefik, U. Wiesner, O. Hess, U. Steiner, V. K. Valev, and J. J. Baumberg, "Ultrafast nonlinear response of gold gyroid three-dimensional metamaterials," *Phys. Rev. Applied* **2**(4), 044002 (2014).
3. J. J. Baumberg, J. Aizpurua, M. H. Mikkelsen, and D. R. Smith, "Extreme nanophotonics from ultrathin metallic gaps," *Nat. Mater.* **18**(7), 668–678 (2019).
4. J. Langer, D. Jimenez de Aberasturi, J. Aizpurua, R. A. Alvarez-Puebla, B. Auguie, J. J. Baumberg, G. C. Bazan, S. E. Bell, A. Boisen, and A. G. Brolo, "Present and future of surface-enhanced Raman scattering," *ACS Nano* **14**(1), 28–117 (2020).
5. S. E. Bell, G. Charron, E. Cortés, J. Kneipp, M. L. de la Chapelle, J. Langer, M. Prochazka, V. Tran, and S. Schlucker, "Towards reliable and quantitative surface-enhanced Raman scattering (SERS): From key parameters to good analytical practice," *Angew. Chem. Int. Ed.* **59**(14), 5454–5462 (2020).
6. H. Xu, J. Aizpurua, M. Käll, and P. Apell, "Electromagnetic contributions to single-molecule sensitivity in surface-enhanced Raman scattering," *Phys. Rev. E* **62**(3), 4318–4324 (2000).
7. R. Zhang, Y. Zhang, Z. Dong, S. Jiang, C. Zhang, L. Chen, L. Zhang, Y. Liao, J. Aizpurua, and Y. E. Luo, "Chemical mapping of a single molecule by plasmon-enhanced Raman scattering," *Nature* **498**(7452), 82–86 (2013).
8. R. Adato, A. A. Yanik, J. J. Amsden, D. L. Kaplan, F. G. Omenetto, M. K. Hong, S. Erramilli, and H. Altug, "Ultra-sensitive vibrational spectroscopy of protein monolayers with plasmonic nanoantenna arrays," *Proc. Natl. Acad. Sci. U.S.A.* **106**(46), 19227–19232 (2009).
9. K. Chen, R. Adato, and H. Altug, "Dual-band perfect absorber for multispectral plasmon-enhanced infrared spectroscopy," *ACS Nano* **6**(9), 7998–8006 (2012).
10. T. B. Hoang, G. M. Akselrod, C. Argyropoulos, J. Huang, D. R. Smith, and M. H. Mikkelsen, "Ultrafast spontaneous emission source using plasmonic nanoantennas," *Nat. Commun.* **6**(1), 7788 (2015).
11. T. P. Sidiropoulos, R. Röder, S. Geburt, O. Hess, S. A. Maier, C. Ronning, and R. F. Oulton, "Ultrafast plasmonic nanowire lasers near the surface plasmon frequency," *Nat. Phys.* **10**(11), 870–876 (2014).
12. A. Frisk Kockum, A. Miranowicz, S. De Liberato, S. Savasta, and F. Nori, "Ultrastrong coupling between light and matter," *Nat. Rev. Phys.* **1**(1), 19–40 (2019).
13. A. Xomalis, R. Chikkaraddy, E. Oksenberg, I. Shlesinger, J. Huang, E. C. Garnett, A. F. Koenderink, and J. J. Baumberg, "Controlling Optically Driven Atomic Migration Using Crystal-Facet Control in Plasmonic Nanocavities," *ACS Nano* **14**(8), 10562–10568 (2020).
14. J. J. Baumberg, "Picocavities: a Primer," *Nano Lett.* **22**(14), 5859–5865 (2022).
15. E. Cortés, "Activating plasmonic chemistry," *Science* **362**(6410), 28–29 (2018).
16. L. Zhou, D. F. Swearer, C. Zhang, H. Robotjazi, H. Zhao, L. Henderson, L. Dong, P. Christopher, E. A. Carter, and P. Nordlander, "Quantifying hot carrier and thermal contributions in plasmonic photocatalysis," *Science* **362**(6410), 69–72 (2018).
17. A. Xomalis, X. Zheng, R. Chikkaraddy, Z. Koczor-Benda, E. Miele, E. Rosta, G. A. Vandenbosch, A. Martínez, and J. J. Baumberg, "Detecting mid-infrared light by molecular frequency upconversion in dual-wavelength nanoantennas," *Science* **374**(6572), 1268–1271 (2021).
18. H. Zong, C. Yurdakul, Y. Bai, M. Zhang, M. S. Unlu, and J.-X. Cheng, "Background-suppressed high-throughput mid-infrared photothermal microscopy via pupil engineering," *ACS Photonics* **8**(11), 3323–3336 (2021).
19. Q. Xia, J. Yin, Z. Guo, and J.-X. Cheng, "Mid-infrared photothermal microscopy: principle, instrumentation, and applications," *J. Phys. Chem. B* **126**(43), 8597–8613 (2022).
20. Y. Zhang, H. Zong, C. Zong, Y. Tan, M. Zhang, Y. Zhan, and J.-X. Cheng, "Fluorescence-detected mid-infrared photothermal microscopy," *J. Am. Chem. Soc.* **143**(30), 11490–11499 (2021).
21. Y. Bai, Z. Guo, F. C. Pereira, M. Wagner, and J.-X. Cheng, "Mid-Infrared Photothermal-Fluorescence in Situ Hybridization for Functional Analysis and Genetic Identification of Single Cells," *arXiv*, arXiv:2209.03741 (2022).
22. R. Chikkaraddy, R. Arul, L. A. Jakob, and J. J. Baumberg, "Single-molecule mid-IR detection through vibrationally-assisted luminescence," *arXiv*, arXiv:2205.07792 (2022).
23. A. Xomalis, X. Zheng, A. Demetriadou, A. Martínez, R. Chikkaraddy, and J. J. Baumberg, "Interfering Plasmons in Coupled Nanoresonators to Boost Light Localization and SERS," *Nano Lett.* **21**(6), 2512–2518 (2021).
24. A. Lombardi, M. K. Schmidt, L. Weller, W. M. Deacon, F. Benz, B. de Nijs, J. Aizpurua, and J. J. Baumberg, "Pulsed Molecular Optomechanics in Plasmonic Nanocavities: From Nonlinear Vibrational Instabilities to Bond-Breaking," *Phys. Rev. X* **8**(1), 011016 (2018).
25. F. Benz, M. K. Schmidt, A. Dreismann, R. Chikkaraddy, Y. Zhang, A. Demetriadou, C. Carnegie, H. Ohadi, B. De Nijs, and R. Esteban, "Single-molecule optomechanics in "picocavities"," *Science* **354**(6313), 726–729 (2016).
26. P. Roelli, D. Martin-Cano, T. J. Kippenberg, and C. Galland, "Molecular Platform for Frequency Upconversion at the Single-Photon Level," *Phys. Rev. X* **10**(3), 031057 (2020).